HOSTED BY
ELSEVIER
Available online at www.sciencedirect.com
ScienceDirect
Soils and Foundations 64 (2024) 101424
www.elsevier.com/locate/sandf

Technical Paper

The effects of internal erosion on granular soils used in transport embankments

I. Johnston [a,b,*], W. Murphy [a], J. Holden [b]

[a] School of Earth and Environment, University of Leeds, Leeds LS2 9JT, UK
[b] water@leeds, School of Geography, University of Leeds, Leeds LS2 9JT, UK

Received 28 April 2023; received in revised form 14 December 2023; accepted 4 January 2024

Abstract

The flooding of embankments used for rail and other infrastructure has the potential to cause lasting weakening of slopes via the movement of fine particles induced by seepage. In laboratory experiments, internal erosion was induced in granular soil samples, with properties consistent with those used to construct transportation embankments, to assess how particle migration through, and out of, samples caused shear wave velocity, strength, stiffness and permeability changes. Shear wave velocity changes, measured using horizontal bender elements, of up to 19 % were observed following fine particle removal of up to 1 % of initial sample mass. Shear wave velocity change was found to be an indicator for identifying the development of permeability change during seepage-induced particle migration. Median measured permeability changes were +5 % and −34 % for samples containing 15 % and 30 % fines, respectively. The largest directly observed permeability and shear wave velocity changes occurred during the initial stages of seepage. Negative correlation was observed between mass of material removed from samples and peak friction angle. Following seepage, soils displayed a dual stiffness behaviour. Stiffness and strength changes were attributed to redistribution of fine particles and opening of pore spaces. Our results have implications for the monitoring of earthworks affected by flooding and seepage as the associated redistribution of fine particles may lead to large changes in slope properties.

Keywords: Suffusion; Bender elements; Embankment; Flooding; Seepage; Stiffness; Rail infrastructure; Internal erosion; Soil; Sand

1. Introduction

Failures in transport embankments due to flooding are relatively common (e.g. Tsubaki et al., 2017, Polemio and Lollino, 2011) and have been associated with several fatalities (Mossa, 2007). Although transport embankments are often not designed for flood retention, flooding behind linear infrastructure embankments occurs as they can act as barriers to runoff along the base of slopes and across alluvial floodplains (e.g. Mossa, 2007, Bennett, 1884). With increases in extreme rainfall events and flooding expected under climate change (Field et al., 2012, Tabari, 2020), understanding the impact of flooding on slope-forming material properties and increasing the resilience of embankments to flooding will become ever more important, especially in areas with ageing infrastructure. Seepage can affect the strength of the material and therefore has an impact on mid to long term embankment stability (Sato and Kuwano, 2016). In addition to changes in strength and soil behaviour, characteristic changes in shear modulus throughout an embankment may create localised instability during dynamic loading applied by high-speed trains on rail infrastructure. Given the global expansion of high-speed rail, and expected increases in extreme weather and flooding (Dodman et al., 2022, Field et al., 2012), it is

* Corresponding author.
E-mail address: i.g.johnston@leeds.ac.uk (I. Johnston).

https://doi.org/10.1016/j.sandf.2024.101424

important to understand processes which can impact on embankment stability over the whole asset lifespan.

Flooding can cause enhanced head development along an embankment which may, in turn, enhance seepage flow through the embankment. Seepage-driven destabilisation can cause failure through sliding or internal erosion-driven weakening (Polemio and Lollino, 2011), which highlights the importance of this process for infrastructure engineering. There is a dearth of studies which consider geotechnical hazards associated with seepage processes during and after flood events around embankments. Embankment failure may not occur in the immediate aftermath of the flood, as seepage-driven processes may cause weakening which allows for a later trigger (Johnston et al., 2021). Therefore, it is important to be able to measure changes in slope strength, stiffness and behaviour following flooding, particularly where internal erosion processes have occurred due to seepage processes.

There are three main types of internal erosion; i) suffosion and suffusion, ii) soil piping and backwards erosion and iii) contact erosion (Bonelli et al., 2007, USBR, 2015, ICOLD, 2017). Here, we focus primarily on suffosion and suffusion, which are the erosion of fine soil particles due to seepage flow with and without volume change respectively (Fannin and Slangen, 2014), due to their ability to alter embankment properties without visible deterioration. Materials susceptible to suffosion and suffusion are said to be internally unstable. Following the removal (washing out) of fine particles, changes have been shown to occur in soil properties including strength, void ratio, small strain stiffness and permeability (Kelly et al., 2012, Chang and Zhang, 2011, Parekh, 2016). Internal stability criteria can be used to assess the internal stability of soils based on grain size distribution (Kenney and Lau, 1985, Kenney and Lau, 1986). Commonly used stability criteria are shown in Table 1. For soils or earthworks to be susceptible to suffosion or suffusion, fine-grained particles must fit through pore spaces in the matrix between coarse-grained particles. The proportion of fine-grained particles must also be low enough so that fines do not fill voids between coarse-grained particles, causing fines loading and preventing particle migration (Wan and Fell, 2008). Chang and Zhang (2013) showed that approximately 20 % and 35 % fines content is needed for fines loading to develop in well graded and gap graded soils, respectively.

Internal erosion can develop when a hydraulic gradient is induced across a sample, or slope, with strong enough seepage forces to cause fine particle movement (Wan and Fell, 2008). Triaxial tests (e.g. Chang and Zhang, 2011, Sato and Kuwano, 2016, Luo et al., 2013) show peak sample strength reduction and development of contractional soil behaviour during shearing following particle loss from internal erosion. In addition, initial increases in sample permeability have been shown to occur as washout is initiated, with subsequent reductions in permeability when clogging of basal soil pores develops (Chang and Zhang, 2011, Ke and Takahashi, 2014, Fannin and Moffat, 2006). Greater losses of fine particles occur in the upstream areas of samples. Migrations of material have been measured in simplified embankment models, with sizes in the range of decimetres (Horikoshi and Takahashi, 2015, Johnston et al., 2023).

Surface wave monitoring of model embankments in laboratory settings has indicated deterioration of embankment properties subject to seepage, with surface wave velocity reductions of up to 30 % attributed to pore pressure increases and effective stress reductions (Planès et al., 2016). In field environments, seasonal variations in surface wave velocity have been measured and attributed to variations in embankment saturation and pore water pressure (Gunn et al., 2018, Bergamo et al., 2016). In addition to short-term moisture-controlled variations in soil properties, it is important to understand permanent changes in material properties - for example caused by seepage-induced particle movement, which likely causes deterioration of earthworks (Sato and Kuwano, 2016). Studies assessing changes in soil stiffness and shear wave velocity (V_s) following particle loss are limited. In laboratory-scale testing, fine particle presence in pore fluids has been shown to increase sample stiffness due to deposition of fine particles onto the contacts of larger grains in soils composed of glass beads (Alramahi et al., 2010). Ben-

Table 1
Instability criteria to identify soils susceptible to internal instability.

Author	Criteria
Kezdi (1979)	$D^c_{15}/D^f_{85} < 4$, material is considered internally stable.
Kenney and Lau (1985)	$h/f > 1.3$ = stable
	$h/f < 1.3$, transition
	$h/f < 1$, unstable
Wan and Fell (2008)	Transition zone: $15/\log(D_{20}/D_5) < 22$ and $30/\log(D_{90}/D_{60}) > 80$
	Unstable zone: $15/\log(D_{20}/D_5) < 15$ and $30/\log(D_{90}/D_{60}) > 110$
	Unsuitable for fines < 15 %
Indraratna et al. (2011)	Stable zone: $D^c_{35}/d^f_{85} < 0{:}73$
	Transition zone: $0.73 \leq D^c_{35}/d^f_{85} \leq 0{:}82$
	Unstable zone: $D^c_{35}/d^f_{85} > 0{:}82$

Dx – size of sieve which passes x% of a soil sample by weight. D^f_x refers to the fine soil fraction, D^c_x refers to the coarse soil fraction. f is the weight fraction finer than grainsize d. h is the weight fraction between grainsize d and 4d, where d is specified by the user.

der elements have been used to identify changes in V_s following changes in localised effective stress (Parekh, 2016) and following dissolution of salt fines, used as a proxy for internal erosion, with V_s reductions of up to 26 % (Truong et al., 2010) and 40 % (Kelly et al., 2012) recorded. However, we are not aware of studies assessing changes in V_s in samples undergoing internal erosion.

We sought to test how strength, shear wave velocity and permeability change in granular embankment materials subject to seepage forces, for two fines contents typical of those used in embankment construction. In particular, we sought to determine the degree to which internal fine particle movement led to changes in sample shear wave velocity, stiffness, permeability and strength, due to the removal of fines from pore spaces, fines redeposition and downstream accumulation, and the removal of fines from samples. We aimed to assess whether these processes were enhanced for larger hydraulic heads and for longer time periods under flood simulation. To support our assessment, we measured changes in sample V_s, using micro seismic techniques during seepage flow, and mass of outflow sediment.

2. Methods

Internal erosion testing was undertaken on soils with fines contents of 15 % and 30 % in a flexible skinned triaxial cell. Strength, permeability, shear wave velocity and particle loss were monitored during testing. V_s measurement was undertaken using horizontal bender elements. Horizontal bender elements were used because vertical elements would only show V_s change following complete particle removal. Horizontal bender elements measure change perpendicular to the flow direction, which allowed for monitoring of material movement during seepage. Shear waves were used in this context as they allowed for near continuous monitoring of change. Additionally, the same parameters control surface waves and shear waves. Therefore, there is a direct link to two of the geophysical methods used for embankment monitoring (Gunn, 2011). Eight seepage tests with shearing were undertaken for each fines content. A control test which was saturated, consolidated and sheared but without seepage, was undertaken to assess whether any material washout occurred due to the testing procedure and this was undertaken on a sample containing 30 % fines. Additional seepage tests without shearing were undertaken in samples containing fluorescein powder on the top surface to track seepage front development. Fluorescein testing was undertaken on samples with both 15 % and 30 % fine material content. In samples containing fluorescein, seepage was halted when fluorescent water first exited samples, to prevent dilution of fluorescein to unobservable levels, and these samples were not sheared to avoid disrupting seepage pathways. Tests undertaken on samples containing fluorescein are not listed in Table 2. Test duration (d) and hydraulic gradient (i) were varied between tests.

2.1. Sample material

Sample soils were comprised of sub-rounded to angular sands and silt. Sieving was used to split bulk samples, comprising sharp sands and river sands, into 12 bands between 43 μm and 2 mm. Material from individual grain size bands were then combined to create a bulk soil with the desired grain size distribution (Fig. 1), from which material was taken for each test. The grain size distributions of soil mixes were formed to meet UIC 719R – the specification for high-speed rail embankment material given by the International Union of Railways – which stipulates $Cu > 6$ (Eq. (1)) and $1 < Cc < 3$ (Eq. (2)):

$$Cu = D_{60}/D_{10} \tag{1}$$

$$Cc = D_{30}^2/(D_{10}D_{60}) \tag{2}$$

where Cu is the coefficient of uniformity, Cc is the coefficient of curvature, and D_x is the grainsize at a given grainsize distribution percentile. Soil 'fines' were categorised as those <125 μm and were non-plastic. Fines contents of 15 % and 30 % were used for the two sets of tests undertaken (Fig. 1). The 15 % and 30 % fines material had optimum moisture contents of 14.2 % and 9.5 % and maximum dry densities of 2.10 g/cm^3 and 2.13 g/cm^3, respectively. Though the soils used in these samples meet the UIC 719R specification for high-speed rail embankment materials for modern rail embankments, they are likely more representative of older embankments and those designed without the specific purposes of water retention. More modern slopes, and those designed to withstand water impoundment, are likely to be constructed of materials with smaller gap ratios and therefore less susceptible to internal erosion processes (Chang and Zhang, 2013).

Samples were prepared via moist compaction with a 5 % moisture content, using de-aired water, to prevent fines separation during preparation (Kwan and Mohtar, 2018). Samples were prepared inside a metal split mould and tested inside a flexible latex membrane. Seven lifts with decreasing thicknesses were used during the construction of individual samples to prevent overcompaction. During each lift, a funnel was used to minimise the drop height of soil to prevent soil segregation. Samples were 100 mm high × 50 mm diameter. Sample material was well graded and categorised as unstable by the stability indices listed in Table 1. Initial sample properties and test conditions are shown in Table 2.

2.2. Testing apparatus

Testing was undertaken in a Wykehan Farrance triaxial system modified to include horizontally-orientated bender elements (e.g. Pennington et al., 1997), vertical fluid flow

Table 2
Initial sample properties and test properties for samples which underwent seepage and shearing.

Test	Density (g/cm^3)	Initial K (m/s^1 x10^{-7})	*Initial* (V_s, m s^1)	Hydraulic gradient (i)	Seepage duration (mins)	Water seepage volume (cm^3)	B value	Confining pressure during shear (kPa)	Back pressure during shear (kPa)
15A	1.74	37.9	302	3	299	1110	0.88	60	30
15B	1.62	34.9	384	3	100	1200	0.93	66	27
15C	1.73	11.3	284	3	348	120	0.88	60	25
15D	1.68	35.8	387	3	132	1570	0.92	66	30
15E	1.68	44.4	309	3	88	1000	0.89	66	39
15F	1.89	45.1	474	5	91	1200	0.87	62	22
15G	1.76	4.6	428	5	267	860	0.91	60	27
15H	1.72	21.6	370	3	184	2240	0.87	52	30
30A	1.80	339	243	3	100	1260	0.88	56	40
30B	1.81	21.0	203	5	106	1390	0.94	56	40
30C	1.84	39.5	234	5	206	1800	0.86	70	48
30D	1.81	37.1	218	3	200	1400	0.87	70	30
30E	1.82	12.6	235	3	51	30	0.85	67	30
30F	1.83	230	204	5	50	650	0.93	70	50
30G	1.53	–	–	–	0	0.00	0.93	70	30
30H	1.72	21.6	143	3	250	2804	0.86	70	30

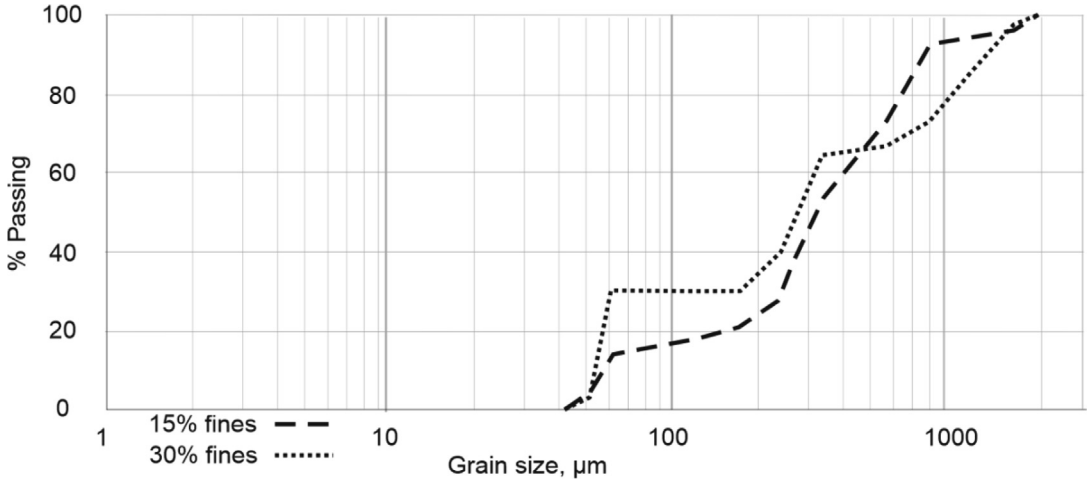

Fig. 1. Grain size distribution for the soils tested.

through samples and washout collection (Fig. 2). Bender elements, associated oscilloscope systems, control and sampling software were constructed by VJ-TECH (Product IDs VJT0265-HRZ and VJT-csBEND). Bender element insertion has not been found to alter the shear strength of granular materials during triaxial testing (e.g. Salgado et al., 2000). De-aired water flow through samples was controlled by a pump with volume accuracy of +/-1 mm^3, pressure accuracy +/-1 kPa and a volume of 200 cm^3. The basal platen consisted of a 1 mm thick steel mesh with 1 mm circular holes and 2 mm pitch to allow for fines migration from the base of samples while supporting the coarse fraction of the sample. Tubing around the outside of the mesh prevented the blocking of mesh pores and base densification. A porous plate was used at the top of the sample to ensure water distribution from the flow input across the sample area.

Bender elements were inserted horizontally across the middle of the samples after the samples were removed from the mould. Liquid latex sealant was used to ensure sample isolation from confining pressure water. Bender elements had an 11 mm wide, 4 mm deep and 2 mm high intrusion into samples. Wave travel times were measured using the peak to peak time domain method (Fig. 3) to remove error associated with picking first arrivals caused by the near-field effect and P wave reflections (Yamashita et al., 2007). The distance between elements was taken as the tip to tip distance, after Yamashita et al. (2009). Wave frequencies of 30 or 50 kHz were used during tests on samples with 15 % fines content and 10 or 15 kHz during tests with 30 % fines content; lower frequency waves were utilised in samples where the initial higher frequency wave did not produce an observable output signal. Input signals were

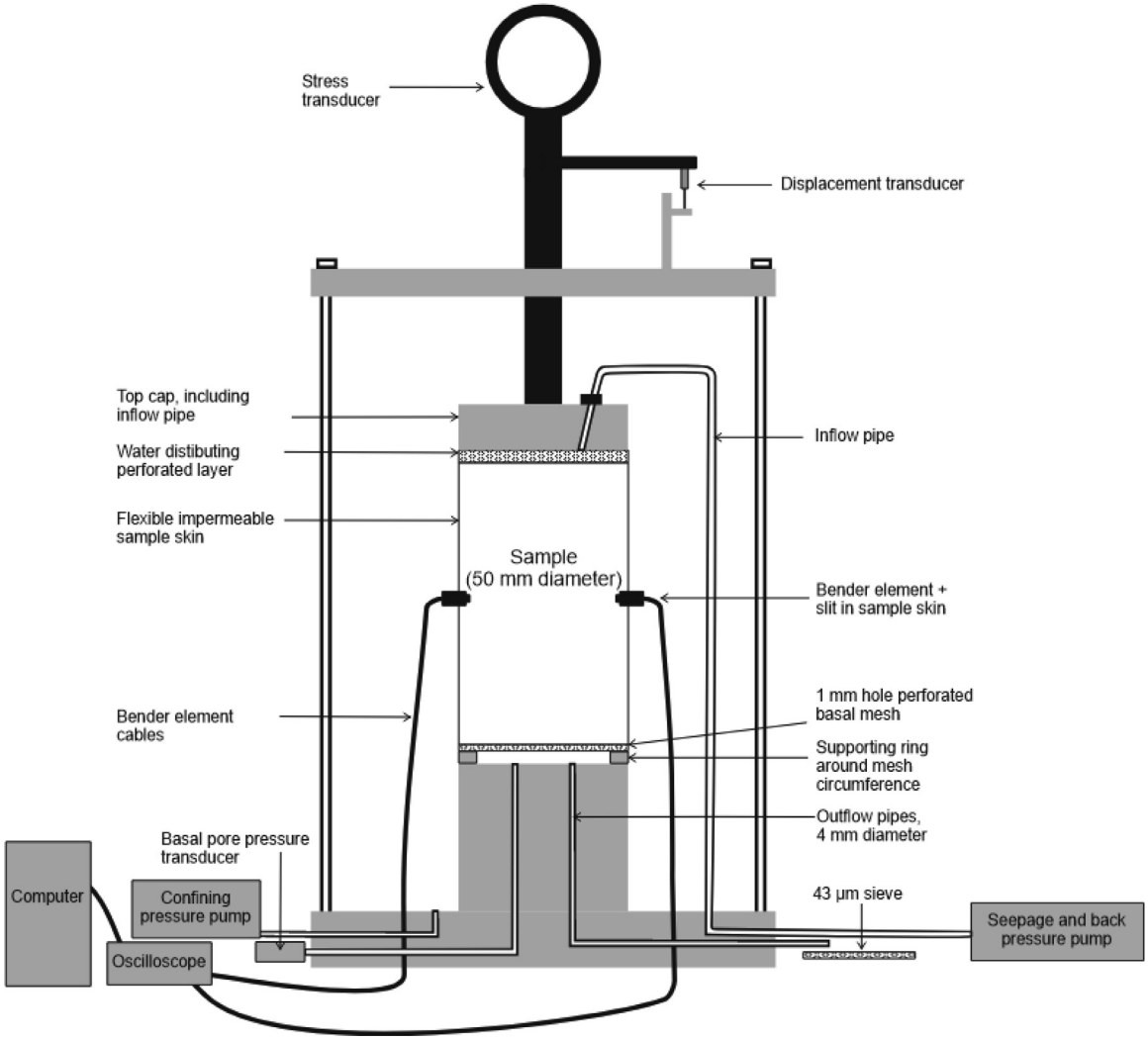

Fig. 2. Experimental apparatus for bender element and seepage modified triaxial tests.

sent as individual sinewave pulses, with readings taken every 2–3 minutes during seepage. Signal stacking was utilised for all readings to reduce signal noise. Shear wave veloities measured using the bender elements had an error of +/- 1.0 m s^{-1}.

2.3. Seepage and shearing

The seepage and triaxial testing processes incorporated four main stages: 1) Saturation and consolidation; 2) Seepage; 3) Shearing; 4) Material collection.

2.3.1. Saturation and consolidation

Samples underwent isotropic consolidation and saturation prior to the initiation of seepage. Back pressure was gradually increased to minimise particle disturbance prior to seepage. Minimum B-values of 0.85 were achieved during saturation; though below the recommended B-value of 0.95 in BS EN 17892:2018, further increases in confining pressure did not produce increases in B value so saturation was considered complete (British Standards Institution, 2018). Back pressure was not maintained during seepage, as the base of samples was open to atmospheric pressure.

2.3.2. Seepage stage

After consolidation, seepage through samples was undertaken for different durations of seepage (Table 2) and consisted of pressurised downwards seepage flow using de-aired tap water with hydraulic gradients (i) of 3 or 5 (Table 2). Tests with similar seepage durations were tested with different hydraulic gradients (e.g. tests 30A and 30B, 30E and 30F) to identify potential effects of hydraulic gradient variation on sample behaviour. As washout mass could only be recorded at the end of tests, seepage durations were chosen to provide a range of endpoints, to identify potential relationships between seepage and washout mass.

Seepage was non-continuous and ~200 cm^3 of water flowed through samples before a period of zero flow while the pump was refilled. The refilling period lasted approximately eight minutes. Recorded seepage times do not include the refilling period. During refilling, cell drainage

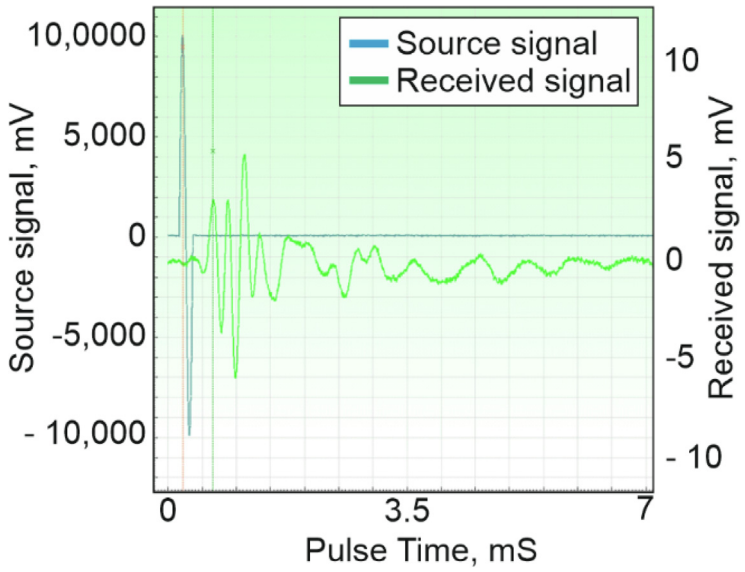

Fig. 3. Example of peak-to-peak shear wave velocity measurement. Transmitted and received peaks are shown by vertical dashed lines.

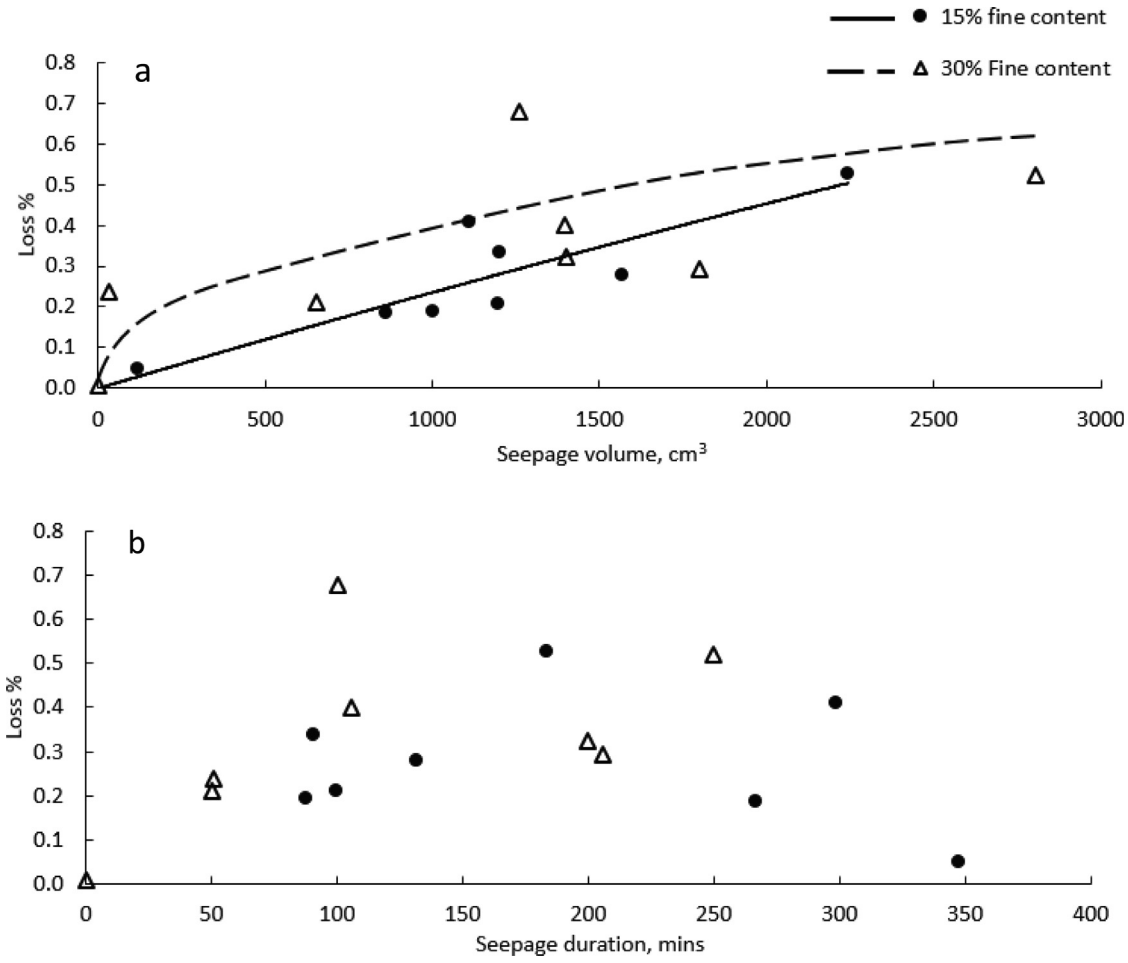

Fig. 4. Mass of material washed out from samples during seepage recorded against a) seepage volume and b) seepage duration.

taps were closed to maintain sample condition and, during seepage, sample saturation was maintained by ensuring the outflow pipe was above the height of the sample base.

During the seepage stage, permeability (in this case saturated hydraulic conductivity, K) and V_s were measured every 2–3 min; pre-seepage shear wave velocity values

(Table 2) were measured post-consolidation and before seepage starting. Wave frequency was kept constant throughout individual tests to prevent alteration of V_s readings. Initial K values are equal to the first K measurement during seepage. In tests D and E, K and V_s measurements had longer return periods. Permeability was calculated by measuring the volume of water entering samples over time with a given hydraulic gradient.

2.3.3. Shearing stage

Following seepage, back pressure and confining pressure were reimposed prior to the initiation of consolidated drained shearing. During the drained shear stage, loading was rate controlled. The loading rate specified on the load frame ensured pore water pressure increases did not occur within samples and did not exceed 10 % per hour, as specified by BS EN ISO 17892-9:2018 British Standards Institution (2018). Effective stress values were chosen to represent conditions found in embankments, with values primarily representative of materials in the upper 3–6 m of embankment bodies. As pressures were maintained by individual pumps and on-cell pressure transducers, rather than a centralised computer system, coupled with the relatively low pressures used in the tests, maintaining exact pressures between tests was not possible.

Due to the necessity of altering pore water pressures and confining pressures during testing, effective stress changes developed within samples during the testing process. Increases in effective stress, after seepage through samples was complete, had the potential to alter, through compression, the soil structure created by particle movement. While increases in pore water pressures are likely to occur on embankment slopes in field environments, significant changes in confining pressure are unlikely to occur. Therefore, material compression is less likely to occur in full scale embankments.

2.3.4. Material collection

Following shearing, samples were disassembled and any material washed out of the sample which had remained in the testing cell outflow pipes was collected, in addition to material which had been collected in the 43 μm outflow sieve. As material remained within the testing cell during seepage, it prevented the continuous monitoring of washed out material mass.

3. Results

3.1. Particle removal

Particle loss and volume of seepage water were very strongly positively correlated in samples containing 15 % fines content, ($r = 0.878$, $p = 0.001$) and moderately positively correlated in samples containing 30 % fines content ($r = 0.626$, $p = 0.05$) (Fig. 4a). Discoloured water, which became paler with additional seepage, was observed exiting the sample cell throughout the duration of the tests, providing qualitative evidence that material migration was prevalent throughout the majority of test durations. In all tests, the majority (>60 %) of particles that were washed out from samples were <125 μm with 67 % or more of particles < 210 μm. The removal of mass per cross sectional sample area per litre of seepage water (g $m^{-2}L^{-1}$) reduced with increasing seepage volume (Table 3). A total of 0.03 g (<0.01 %) of material was removed from sample 30G, which underwent the saturation and shearing processes but not seepage, representing the washout mass loss caused by non-seepage processes during testing (Table 3). Seepage duration and washed out material mass were not correlated (Fig. 4b). For all samples, the percentage of particles removed from samples by mass lies within a 95 % confidence interval. Sample volume change was not observed during seepage, as additional confining pressure

Table 3
Soil property changes comparing before and after seepage tests. For *Vs* and K change, negative values indicate a reduction after seepage. % changes are relative to initial values.

Test	V_s change (m/s^1)	V_s change (%)	K change (m/s^1 x 10^{-7})	K change (%)	Friction angle (°)	Loss ($g/m^{-2}(-\|-)$ L^{-1})	Total loss (g)	Total loss (%)
15A	−4.6	−1.5	−26.4	−70	22	0.610	1.33	0.41
15B	0.10	0.0	2.5	+7	27	0.292	0.69	0.21
15C	0.0	0.0	−10.2	−90	43	0.696	0.16	0.05
15D	−0.7	−0.2	3.5	+10	33	0.303	0.94	0.28
15E	21	6.7	−1.7	−4	26	0.328	0.64	0.19
15F	2.7	0.6	1.1	+3	38	0.480	1.13	0.33
15G	−16	−3.7	0.4	+9	21	0.384	0.65	0.19
15H	−4.6	−1.2	3.0	+14	21	0.424	1.86	0.53
30A	18	7.5	87.1	+26	12	0.980	2.43	0.68
30B	−3.2	−1.6	25.1	+120	19	0.519	1.38	0.40
30C	44	19.0	−17.7	−45	29	0.293	1.02	0.29
30D	−1.5	−0.7	−24.1	−65	30	0.431	1.15	0.32
30E	−2.0	−0.9	−11.2	−88	31	12.684	0.81	0.24
30F	−1.1	−0.5	−12.1	−5	22	0.545	0.72	0.21
30G	–	–	–	–	28	–	0.03	0.01
30H	6.7	4.7	−151.0	−34	32	0.312	1.72	0.52

water was not added to the cell and confining pressure drops were not observed during seepage.

3.2. Shear wave velocity change

Total V_s change in samples over the full duration of tests was not related to particle mass loss or seepage volume. During seepage, V_s change predominantly occurred over short time periods during the initial phases of seepage (Fig. 5). More gradual V_s changes were observed during prolonged seepage. V_s variations frequently occurred in tandem with changes in sample permeability (Fig. 5). For the full test durations, V_s increases and decreases greater than measurement error were recorded in five and eight tests, for 15 % and 30 % fines respectively (Table 3; Fig. 5). Maximum recorded V_s change was 19 % of initial V_s. More commonly, full test duration V_s changes ranged from 0 to 7 % of initial V_s (Table 3) with similar magnitudes found for tests with 15 % and 30 % fines content.

3.3. Drained shear strength and stiffness

During post seepage drained shearing, a negative correlation was observed between the amount of material removed from samples during seepage and the peak friction angle (ϕ) in samples with 15 % and 30 % fines content. Increased amounts of material removed from samples caused reductions in friction angle (Fig. 6). All post-seepage friction angle values lie within a 95 % confidence interval, except for those from sample 15E. Samples primarily displayed strain hardening behaviour during shear (Fig. 7). At low strains, <1%, strain softening was temporarily observed in the majority of samples prior to the resumption of strain hardening behaviour. Prior to this initial strain softening, samples had higher stiffness, before reloading with lower stiffness (Fig. 7). Samples comprising 15 % fines were sheared over a smaller axial strain range than those with 30 % fines content as bender elements were mounted using silicone sealant during these tests, whereas liquid latex was used to seal bender element insertions during tests containing 30 % fines content. Due to failure of the bond between the silicone sealant and the latex membrane during shear induced sample deformation, samples were compromised by confining pressure water. At this point, shearing was halted and further testing on the sample was not possible.

3.4. Permeability change

Permeability changes were greatest during initial seepage, with change rates decreasing later in tests. Permeability changes often occurred in tandem with V_s changes; the synchroneity of permeability-V_s change was more pronounced during the initial seepage period. Absolute values of permeability change varied over three orders of magnitude between tests, with both positive and negative changes observed. Median relative permeability changes of + 5 % and −33.5 % were recorded for 15 % and 30 % fines, respectively. Permeability reduction was more common in tests with 30 % fines than tests with 15 % fines (Table 3).

3.5. Evidence of particle migration

Three main patterns of concordant permeability and shear wave velocity changes were observed during seepage tests (Fig. 5): i) V_s increases and permeability decreases (e.g. test 30D); ii) V_s decreases and permeability decreases (e.g. 30C); iii) V_s increases and permeability increases (e.g. 30B). In samples containing 30 % fines content, permeability and shear wave velocity trends which developed during seepage predominantly displayed continuous increases or decreases in permeability and shear wave velocity (e.g. Fig. 5A, 5C and 5D). In additional samples containing fluorescein powder which were separated after seepage, without shearing, two styles of seepage front were observed: a relatively uniform front across the width of samples, and concentrated seepage along a flow pathway (Fig. 8).

4. Discussion

4.1. Sample alteration during seepage

Changes in material structure caused by the redistribution and removal of fine particles are thought to be the primary cause of V_s and permeability changes measured. The movement of particles results in the blocking and opening of flow pathways, potentially representing the onset of macropore development and subsequent piping, causing localised changes in effective stress, density, moisture content and stiffness. V_s and K change synchronously in the majority of samples (e.g. Fig. 5d, 5f), indicating the presence of a consistent cause of property change. Two methods of particle redistribution are thought to cause V_s and K changes: i) migration of fine particles downwards through, and out of, samples; and ii) redistribution of fine particles from void spaces to interparticle contacts (Chang and Zhang, 2013, Alramahi et al., 2010) (Fig. 9).

Proportionally large early changes in V_s and K, and reducing rates of loss with increased seepage volume, indicate that the majority of particle movement and loss occurred during early seepage. Rapid property alteration during initial stages of seepage may be related to the movement of initially poorly constrained fine particles, which do not form part of a sample's force chain, through flow pathways and/or to constrictions between coarser grained particles. The lack of volume change in samples during seepage suggests that suffusive particle migration was occurring during seepage and that the redistribution of fine particles, as opposed to soil skeletal collapse, caused property alterations. If suffusion occurred in concentrated areas, it may have allowed for the movement of larger particles due to the initial loss of supporting fine particles. The extensive movement of larger particles, in addition to fine

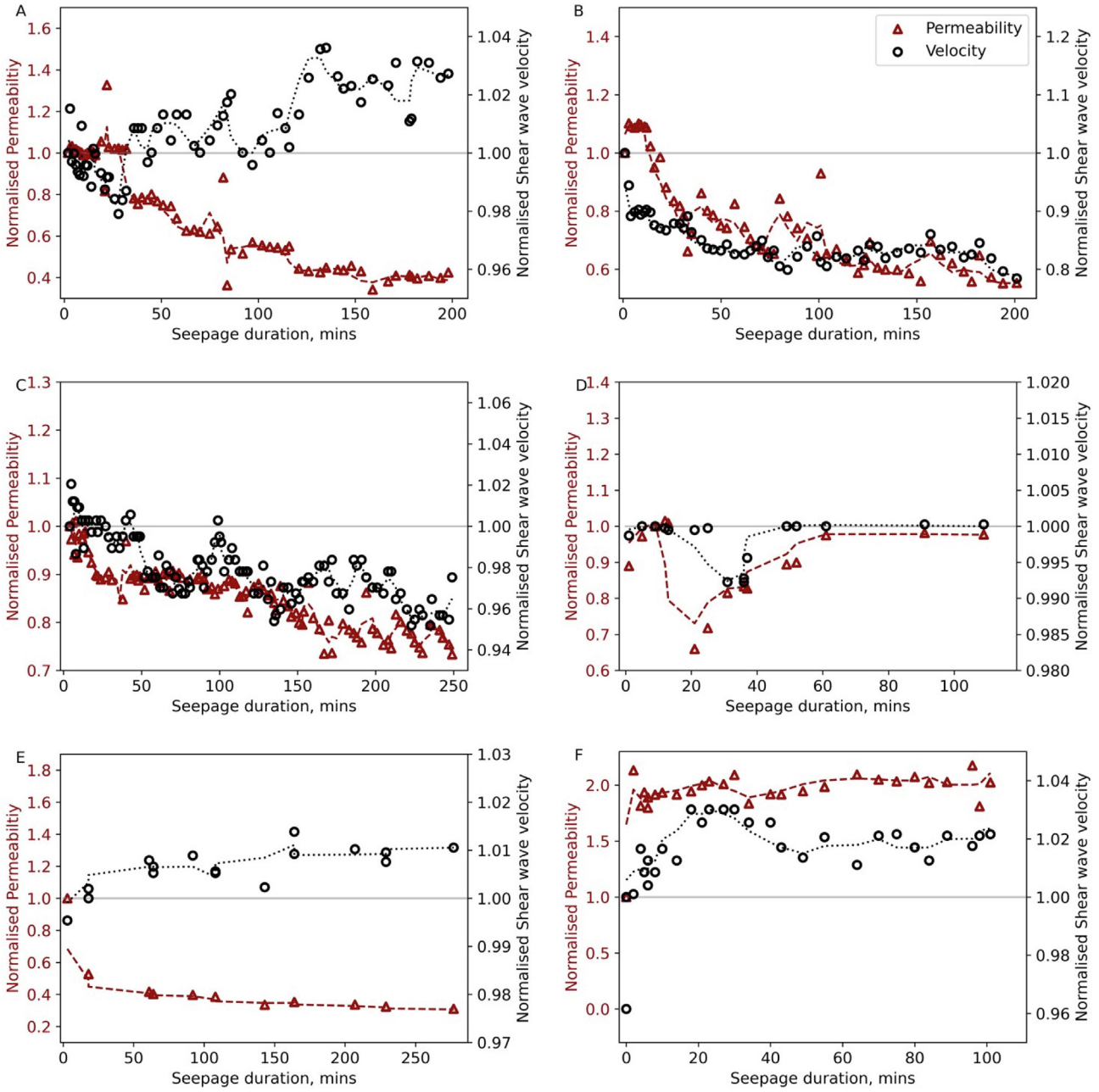

Fig. 5. Observed *Vs* and K over time during seepage for tests a) 30D, b) 30C, c) 30H, d) 15D, e) 15A and f) 30B. d-f are continued over page. Values are normalised by the initial value for the respective property. Trend lines on are three point moving averages.

particles, may have led to the onset of macropore and pipe development.

Shear wave velocity increases are thought to be caused by a greater amount of fine particles entering the V_s measurement zone than were removed (Fig. 9), and by the redistribution of fine-grained particles to coarse-grained particle contacts, when deposition allows for fine-grained particles to accommodate stress transfer (Salgado et al., 2000, Alramahi et al., 2010). A net loss of fine particles from the V_s measurement zone reduces grain interlocking and increases the void ratio, reducing sample density, stiffness and measured V_s (Fig. 9). V_s measurements were point measurements taken in the middle of samples; particle migration outside of this point did not directly affect V_s measurements. Hence, V_s variations are not directly comparable with particle loss. Localised effective stress changes caused by particle migration may also affect V_s measurements (Salgado et al., 2000).

Permeability reductions may have developed in samples where a permeability barrier forms due to the deposition of mobilised particles (Ke and Takahashi, 2014). Samples with continuous increases in K indicate that constrictions, causing particle deposition within the sample, were not present in the zones of samples with the lowest permeability.

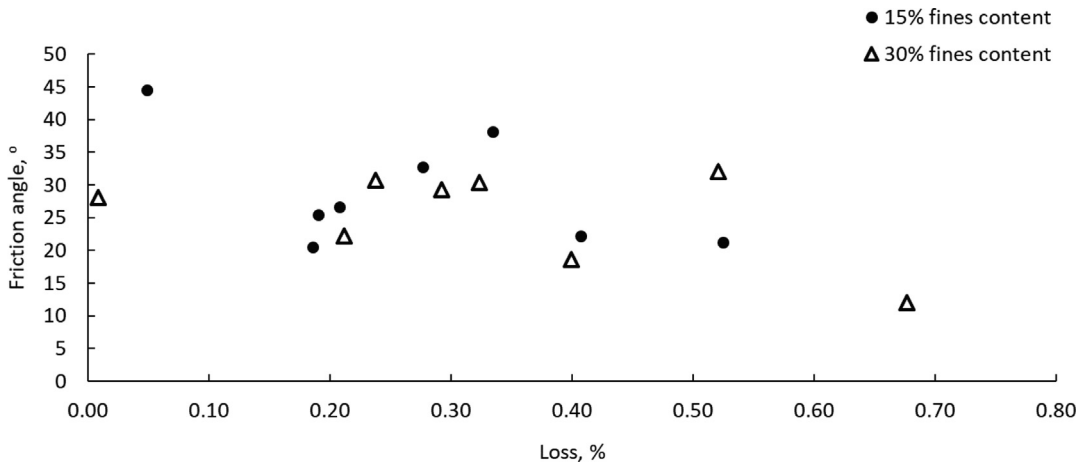

Fig. 6. Friction angle change with percentage of material washed out from samples.

With prolonged duration, observed K reductions were greater. This finding is consistent with internal instability observed by Chang and Zhang (2011); fine particles are deposited within basal pore spaces and clog them during later stage seepage. Relative changes in V_s and K can be used to understand the movement of fine particles within samples. Concordant decreases in V_s and K indicate that there is a net removal of fine particles from the V_s measurement zone and an increase in fine particles in the permeability limiting zone. Increases in V_s and decreases in K indicate that there is densification of the V_s measurement zone. Testing programmes with bender elements at multiple locations, with constant washout mass monitoring, would be needed to define the full nature of particle movement and acoustic velocity changes at higher resolution.

Reducing sediment loss with increased seepage is consistent with multi-stage internal erosion development described by Chang and Zhang (2013). As seepage volume, not duration, is thought to be the primary driver of particle loss we suggest that g m^{-2} L^{-1} should be used when assessing particle loss rate from samples, not g m^{-2} s^{-1}. The decreasing rate of permeability and stiffness change with test progression suggests that the movement of material is focused, although not solely present, in the earlier stages of seepage. This is supported by the visual evidence of outflow water colour becoming paler with test progression. Testing with full continuous monitoring of washed out material is needed to better define the seepage volume–washout relationship. Preferential selection of fine material, below 125 μm, mobilised in samples, shown by the increased mass of washed out finer-grained material, is consistent with grain sizes which the instability criteria (Table 1) denote as unstable.

4.2. Strength behaviour

Variable amounts of particle loss between tests prevented repeat shear testing on a given material. Therefore, peak friction angle was obtained for each sample using the assumption of zero cohesion. The reduction of angle of friction values with increased particle removal is thought to have been caused by the migration of fine particles, creating an overall loosening of the soil structure. Low friction angles recorded in some samples are attributed to the development of loose soil zones following particle loss, e.g. 30A had a friction angle of only 12° and had the highest mass of material removed from the sample. Though reduced sample density and confining pressure during shear have been shown to reduce the peak shear strength of sands (e.g. Chakraborty and Salgado, 2010), these properties were not lower than other tests for sample 30A. Furthermore, no relationship was found between the amount of material removed from samples and initial sample density. The high friction angle of 43° in test 15C is attributed to the long duration of seepage and small mass of material removed from the sample, suggesting that fine particles may have become trapped at interparticle contacts (Alramahi et al., 2010), increasing sample strength.

Samples predominantly displayed strain hardening behaviour during drained shearing (Fig. 7). Low strain, <1%, strain softening is thought to be caused by particle redeposition and intra sample variability. Prior to early-stage strain softening, the stiffness of samples was higher than post strain softening. This is consistent with a behaviour that suggests the initial stress response is representative of a denser, stiffer, material. Following failure, strain hardening resumed with a lower stiffness and represented the looser, weaker, material (Ke and Takahashi, 2015). Angle of friction values are representative of mass failure through less dense, looser zones. Strain softening was not observed in test 30G, undertaken without seepage. Multiple cycles of strain hardening and softening were observed in some samples (e.g. 30B); each successive cycle has lower stiffness than the previous one, suggesting that multiple zones of loose and dense material form during seepage.

While previous research has shown strength reductions and contraction increases following larger amounts of internal erosion development (Sato and Kuwano, 2016,

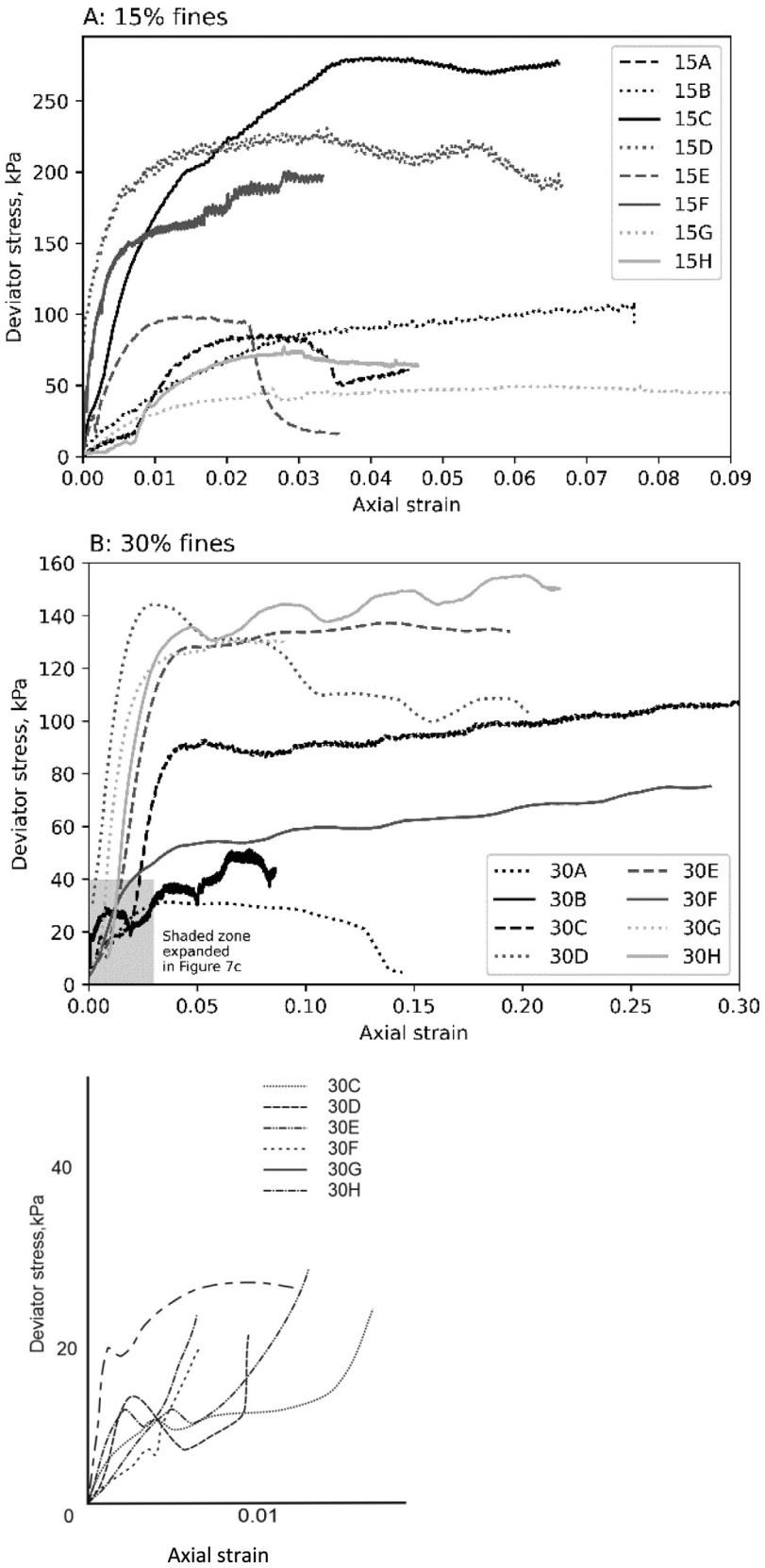

Fig. 7. Shearing curves for tests on samples with (a) 15% and (b) 30% fines content. (c) Shows an enhanced version low strain stress behaviour of samples with 30% fines content. Strains are axial and were measured without on-sample measurement.

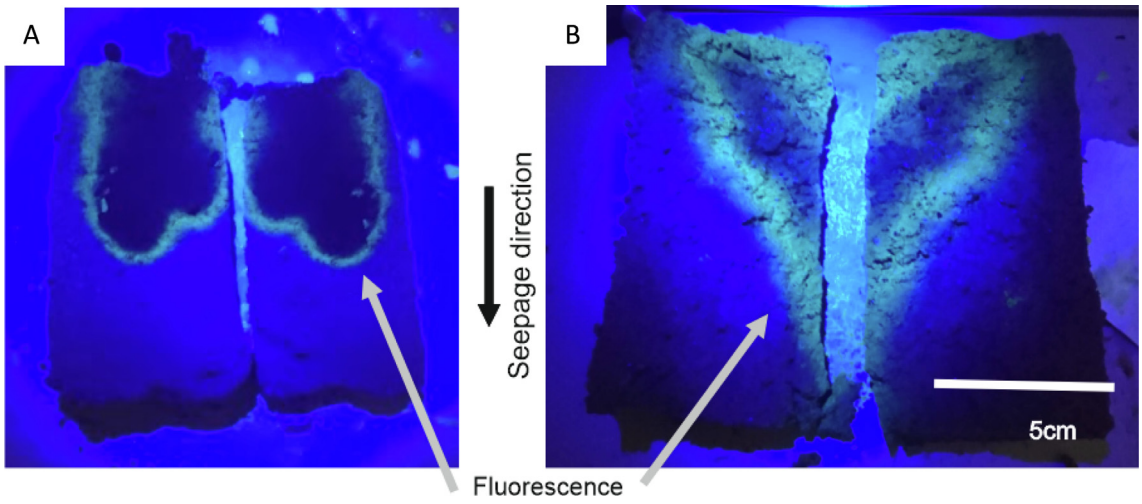

Fig. 8. Seepage front development inside samples shown by fluorescence migration; samples were halved post-seepage and imaged using UV light. Fluorescence was initially located at the top of samples, before migrating downwards during seepage. a) Seepage development across the width of samples. b) Concentrated seepage development along a preferential seepage plane.

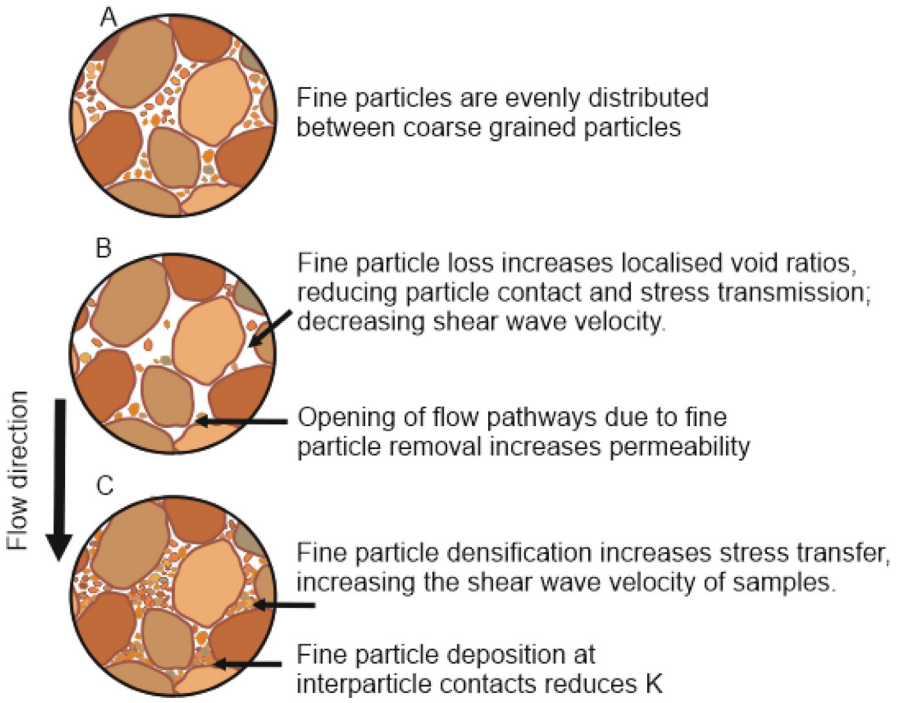

Fig. 9. Conceptual model of change in fine particle distribution and soil structure caused by seepage. A: Prior to seepage. B: Zones of fine particle loss which are thought to cause reduced V_s and increased K. C: Zones of fine particle deposition which are thought to have higher V_s and lower K. The enlargement of pores by fine particle migration can allow for the migration of coarser particles and piping initiation.

Zhang and Cheuk, 2014), no clear pattern was present in our findings. It may be that the proportionally smaller amounts of particle movement and loss which developed during seepage in our tests did not cause strength changes as large as those observed in previous studies, preventing an obvious trend developing.

4.3. Variability

The order of magnitude range of initial permeability values for samples with the same fine particle content (Table 2) is consistent with previous tests which have measured the permeability of compacted granular samples (e.g. Juang

and Holtz, 1986), and all initial permeability values are within two standard deviations of the mean values for 15 % and 30 % fines content samples. The change to soil structure caused by the initial seepage may have altered the initial permeability values from the samples in their constructed condition. Variability in sample structure may also have altered the development of permeability and shear wave velocity changes. Localised sections of samples with higher densities or finer grain sizes may prohibit the movement of fine particles, thus reducing the rates of change in permeability and shear wave velocity observed. The migration of fine particles forms a differential soil structure across samples, resulting in localised behaviour changes.

Variations in the propensity for internal erosion in materials with different levels of saturation have been previously observed (e.g. Zhang et al., 2019), partially due to the potential for preferential flow pathways to develop in unsaturated soils. However, no relationship was found between saturation level and the mass of washed out material recorded in this work. Furthermore, no significant relationship between initial saturation level, density or confining stress and friction angle, mass of particle washout or permeability change was identifed, providing further evidence that the mass of washed out is the cause of altered friciton angles. Absolute V_s changes in the order of 10 % were smaller than V_s reductions recorded by Truong et al. (2010) and Kelly et al. (2012). However, in comparison to the amount of material removed from samples, V_s changes measured in our work (up to ~1 % of initial sample mass) are greater than those recorded by Truong et al. (2010) and Kelly et al. (2012). This suggests that small alterations in material structure through material movement, redeposition and loss (not just full removal of fine particles) can produce significant shear wave velocity, stiffness and permeability changes in soils. Given that flooding events which cause seepage and particle migration have been recorded as causes of slope failure (Polemio and Lollino, 2011), our data show that temporal changes in stiffness and critical velocity of slopes and earthworks need to be considered following flooding along embankments that accelerates seepage through slopes.

4.4. Implications for transportation embankments

Upscaling of laboratory experiments to full embankments remains challenging. However, there are implications for earthworks that should be considered:

1) The formation of flow lines and flow pathways due to particle movement within samples is a possible process by which piping may initiate. Engineers responsible for the management of geotechnical assets should consider inspection of embankments following exposure to significant flood events. Such inspections may utilise walkover surveys or visual inspections to look for evidence of loss of fines, subsidence or evident seepage. However, a lack of visible external alteration does not preclude the potential for material property alteration.
2) The observation that a better correlation exists with flow volume rather than flow duration suggests that short lived, high intensity events may cause greater property changes. The increased intensity of events under climate change (Field et al., 2012) may therefore require increased inspection rates of transport embankments.
3) Geophysical methods using surface waves as a non-invasive means of investigation may need careful planning to capture changes over the embankment. Methods that involve averaging wave velocities over significant volumes of the asset or parallel to the direction of seepage may fail to detect movement of particles and associated material property changes.

5. Conclusions

Horizontal bender element measurements were used to measure changes in granular soil permeability and stiffness caused by seepage flow in a triaxial setting. We found that a total of 1 % of material removal was related to changes in S-wave velocity and permeability of up to 20 %. Increased fine particle loss from samples was shown to cause reduced friction angle. In post seepage shearing, samples were shown to primarily display strain hardening behaviour. However, a dual stiffness was observed – which was attributed to the formation of dense zones of soil caused by fine particle deposition at interparticle contacts. Net permeability reductions over the duration of the experiments were observed in the majority of samples. These changes show the significant potential for seepage through slopes caused by flooding, or other causes, to move earthworks and slopes towards instability. Material property changes and loss were found to be greatest during initial seepage phases. There was little difference in the magnitude of property changes observed between samples with 15 % and 30 % fine particles; samples with greater fines contents displayed more gradual behaviour changes.

Shear wave velocity change appears to be a suitable indicator to help monitor internal erosion onset within samples. Changes in shear wave velocity are found to be concordant with changes in sample permeability when granular soils are subjected to seepage flow which causes particle migration to develop. However, at this stage, a definitive empirical relationship between shear wave velocity change and permeability change has not been idenfieid. Tests with a single shear wave velocity monitoring point are unable to produce V_s measurements which fully quantify the direction, magnitude and causes of mass scale changes in sample property behaviour. Therefore we recommend further testing with a higher resolution array of bender elements to allow full quantification of sample behaviour during seepage.

Acknowledgements

This research has been funded by the UK Natural Environment Research Council and Network Rail as part of the National Productivity Investment Fund award number NE/R009813/1. Laboratory testing was undertaken in the RMEGGh laboratories at the University of Leeds; Kirk Handley is thanked for his help, advice, and assistance during the set up and design of laboratory testing.

References

Alramahi, B., Alshibli, K.A., Fratta, D., 2010. Effect of fine particle migration on the small-strain stiffness of unsaturated soils. J. Geotech. Geoenviron. Eng. 136, 620–628.

Bennett, E. H. 1884. Court of Appeal. Whalley v. Lancashire and Yorkshire Railway Co. The American Law Register (1852-1891), 32, 633–640.

Bergamo, P., Dashwood, B., Uhlemann, S., Swift, R., Chambers, J.E., Gunn, D.A., Donohue, S., 2016. Time-lapse monitoring of climate effects on earthworks using surface waves. Geophysics 81, EN1-EN15.

Bonelli, S., Marot, D., Ternat, F., Benahmed, N., 2007. Assessment of the risk of internal erosion of water retaining structures: dams, dykes and levees.

British standards Institution, 2018. Geotechnical investigation and testing - Laboratory testing of soil. In: COMMITTEE, S. P. A. S. (Ed.) Part 9. BSI Standards Limited.

Chakraborty, T., Salgado, R., 2010. Dilatancy and shear strength of sand at low confining pressures. J. Geotech. Geoenviron. Eng. 136, 527–532.

Chang, D., Zhang, L., 2011. A stress-controlled erosion apparatus for studying internal erosion in soils. Geotech. Test. J. 46 (6), 579–589.

Chang, D.S., Zhang, L.M., 2013. Extended internal stability criteria for soils under seepage. Soils Found. 53, 569–583.

Dodman, D., Hayward, B., Pelling, M., Castan Broto, V., Chow, W.T.L., 2022. Chapter 6: Cities, settlements and key infrastructure. In: Pörtner, H.-O., D.C.R., Tignor, M., Poloczanska, E.S., Mintenbeck, K., Alegría, A., Craig, M., Langsdorf, S., löschke, S., Möller, V., Okem, A., Rama, B. (Ed.) Climate Change 2022: Impacts, Adaptation and Vulnerability. Contribution of Working Group II to the Sixth Assessment Report of the Intergovernmental Panel on Climate Change. Cambridge University Press.

Fannin, R.J., Moffat, R., 2006. Observations on internal stability of cohesionless soils. Géotechnique 56, 497–500.

Fannin, R.J., Slangen, P., 2014. On the distinct phenomena of suffusion and suffosion. Géotechnique Lett. 4, 289–294.

Field, C.B., Barros, V., Stocker, T.F., Dahe, Q., 2012. Managing the Risks of Extreme Events and Disasters to Advance Climate Change Adaptation: Special Report of the Intergovernmental Panel on Climate Change. Cambridge University Press.

Gunn, D.A., Chambers, J.E., Dashwood, B.E., Lacinska, A., Dijkstra, T., Uhlemann, S., Swift, R., Kirkham, M., Milodowski, A., Wragg, J., Donohue, S., 2018. Deterioration model and condition monitoring of aged railway embankment using non-invasive geophysics. Constr. Build. Mater. 170, 668–678.

Gunn, D.A., 2011. Embankment stiffness characterisation using MASW and CSW methods. In: Proc. 11th Int. Conf. Railway Engineering, London.

Horikoshi, K., Takahashi, A., 2015. Suffusion-induced change in spatial distribution of fine fractions in embankment subjected to seepage flow. Soils Found. 55, 1293–1304.

ICOLD 2017. Bulletin 164 Internal Erosion of Existing Dams, Levees and Dikes, and their Foundations. Paris: International Commission on Large Dams.

Indraratna, B., Nguyen, V.T., Rujikiatkamjorn, C., 2011. Assessing the potential of internal erosion and suffusion of granular soils. J. Geotech. Geoenviron. Eng. 137, 550–554.

Johnston, I., Murphy, W., Holden, J., 2021. A review of floodwater impacts on the stability of transportation embankments. Earth Sci. Rev. 215 103553.

Johnston, I., Murphy, W., Holden, J., 2023. Alteration of soil structure following seepage-induced internal erosion in model infrastructure embankments. Transp. Geotech. 42 101111.

Juang, C.H., Holtz, R.D., 1986. Fabric, pore size distribution, and permeability of sandy soils. J. Geotech. Eng. 112, 855–868.

Ke, L., Takahashi, A., 2014. Experimental investigations on suffusion characteristics and its mechanical consequences on saturated cohesionless soil. Soils Found. 54, 713–730.

Kelly, D., Mcdougall, J., Barreto, D., 2012. Effect of particle loss on soil behaviour. In: Proc., 6th Int. Conf. on Scour and Erosion, Publications SHF, Paris, pp. 639-646.

Kenney, T., Lau, D., 1985. Internal stability of granular filters. Can. Geotech. J. 22, 215–225.

Kenney, T.C., Lau, D., 1986. Internal stability of granular filters: Reply. Can. Geotech. J. 23, 420–423.

Kezdi, A., 1979. Soil Physics. Elsevier, Amsterdam.

Kwan, W.S., Mohtar, C.E., 2018. A review on sand sample reconstitution methods and procedures for undrained simple shear test. Int. J. Geotech. Eng. 14, 851–859.

Luo, Y.-L., Qiao, L., Liu, X.-X., Zhan, M.-L., Sheng, J.-C., 2013. Hydro-mechanical experiments on suffusion under long-term large hydraulic heads. Nat. Hazards 65, 1361–1377.

Mossa, M., 2007. The floods in Bari: What history should have taught. J. Hydraul. Res. 45, 579–594.

Parekh, M.L., 2016. Advancing Internal Erosion Monitoring Using Seismic Methods in Field and Laboratory Studies. Colorado School of Mines, Arthur Lakes Library.

Pennington, D., Nash, D., Lings, M., 1997. Anisotropy of G0 shear stiffness in Gault clay. Géotechnique 47, 391–398.

Planès, T., Mooney, M.A., Rittgers, J.B.R., Parekh, M.L., Behm, M., Snieder, R., 2016. Time-lapse monitoring of internal erosion in earthen dams and levees using ambient seismic noise. Géotechnique 66, 301–312.

Polemio, M., Lollino, P., 2011. Failure of infrastructure embankments induced by flooding and seepage: a neglected source of hazard. Nat. Hazards Earth Syst. Sci. 11, 3383.

Salgado, R., Bandini, P., Karim, A., 2000. Shear strength and stiffness of silty sand. J. Geotech. Geoenviron. Eng. 126, 451–462.

Sato, M., Kuwano, R., 2016. Effects of internal erosion on mechanical properties evaluated by triaxial compression tests. Japanese Geotechnical Soc. Special Publication 2, 1056–1059.

Tabari, H., 2020. Climate change impact on flood and extreme precipitation increases with water availability. Sci. Rep. 10, 13768.

Truong, Q.H., Eom, Y.H., Lee, J.S., 2010. Stiffness characteristics of soluble mixtures. Géotechnique 60, 293–297.

Tsubaki, R., Kawahara, Y., Ueda, Y., 2017. Railway embankment failure due to ballast layer breach caused by inundation flows. Nat. Hazards 87, 717–738.

USBR 2015. Best Practices in Dam And Levee Safety Risk Analysis, fourth ed.

Wan, C.F., Fell, R., 2008. Assessing the potential of internal instability and suffusion in embankment dams and their foundations. J. Geotech. Geoenviron. Eng. 134, 401–407.

Yamashita, S., Fujiwara, T., Kawaguchi, T., Mikami, T., Nakata, Y., Shibuya, S., 2007. International parallel test on the measurement of G_{max} using bender elements. Organized by Technical Comittee 29.

Yamashita, S., Kawaguchi, T., Nakata, Y., Mikami, T., Fujiwara, T., Shibuya, S., 2009. Interpretation of international parallel test on the measurement of G_{max} using bender elements. Soils Found. 49, 631–650.

Zhang, L., Cheuk, J., 2014. Mechanical consequences of internal soil erosion AU - Chang, Dongsheng. HKIE Trans. 21, 198–208.

Zhang, D., Du, W., Gao, C., 2019. An experimental investigation of internal erosion around defective pipe in saturated-unsaturated soil. In: 7th Asia-Pacific Conference on Unsaturated Soils. Nagoya City, Japan.